TRENDS IN SCIENCES 2026; 23(10): 13489
https://doi.org/10.48048/tis.2026.13489 RESEARCH ARTICLE

Secretome from Human Umbilical Cord Mesenchymal Stem Cells Ameliorates Ovarian Aging in a Murine Model

Yulice Soraya Nur Intan[1,2], Soetrisno[3,4], Abdurahman Laqif[4], Dono Indarto[3,5,*], Paramasari Dirgahayu[3,6], Eti P. Pamungkasari[3,7] and Agung Putra[8,9,10]

[1]*Student of Doctoral Program in Medical Science, Faculty of Medicine, Universitas Sebelas Maret, Surakarta, Indonesia*
[2]*Department of Obstetrics and Gynecology, Faculty of Medicine, Universitas Islam Sultan Agung, Semarang, Indonesia*
[3]*Doctoral Program in Medical Sciences, Faculty of Medicine, Universitas Sebelas Maret, Surakarta, Indonesia*
[4]*Department of Obstetrics and Gynecology, Faculty of Medicine, Universitas Sebelas Maret / Dr. Moewardi Hospital Surakarta, Indonesia*
[5]*Department of Physiology and Biomedical Laboratory, Universitas Sebelas Maret, Surakarta, Indonesia*
[6]*Department of Parasitology and Mycology, Faculty of Medicine, Universitas Sebelas Maret, Surakarta, Indonesia*
[7]*Department of Public Health, Faculty of Medicine, Universitas Sebelas Maret, Surakarta, Indonesia*
[8]*Department of Pathology Anatomy, Faculty of Medicine, Universitas Islam Sultan Agung, Semarang, Indonesia*
[9]*Stem Cell and Cancer Research Indonesia, Semarang, Indonesia*
[10]*Doctoral Study Program, Faculty of Medicine, Universitas Islam Sultan Agung, Semarang, Indonesia*

([*]Corresponding author's e-mail: dono@staff.uns.ac.id)

Received: 28 January 2026, Revised: 8 March 2026, Accepted: 20 March 2026, Published: 20 May 2026

Abstract

Ovarian aging represents a complex biological process characterized by follicular depletion, hormonal dysregulation, and chronic inflammation. We investigated the therapeutic potential of the secretome derived from human umbilical cord mesenchymal stem cells (S-HUMCMSCs) in naturally aged female mice. Administration of S-HUMCMSCs significantly reduced serum FSH levels (from 5.43 ± 1.59 to 3.07 ± 2.69 mIU/mL, $p < 0.05$), decreased senescent cell percentage (from 27.35 ± 0.82% to 8.37 ± 0.85%, $p < 0.001$), and modulated inflammatory markers with reduction in TNF-α (from 188.23 ± 83.31 to 4.55 ± 4.78 ng/mL, $p < 0.001$) and elevation in IL-10 (7.55 ± 7.77 ng/mL, $p < 0.05$). Additionally, S-HUMCMSCs treatment decreased p53 expression (179.17 ± 170.48 vs. 549.67 ± 243.62 in aged controls, $p < 0.025$) and preserved ovarian follicular architecture. A comparative analysis with 17β-estradiol therapy demonstrated comparable efficacy in improving ovarian parameters. Although no formal toxicological or long-term safety assessments were conducted, no adverse clinical signs or behavioral abnormalities were observed during the study period. These findings establish S-HUMCMSCs as a promising cell-free regenerative approach for managing age-related ovarian dysfunction by modulating multiple pathways involved in senescence, inflammation, and hormonal homeostasis.

Keywords: Secretome, Aging, MSCs, Hormone therapy

Introduction

Reproductive aging in females represents one of the earliest manifestations of systemic senescence, with ovarian function declining substantially before other organ systems show significant age-related deterioration [1]. This premature aging of the reproductive system manifests clinically as perimenopause and menopause, conditions affecting quality of life through vasomotor symptoms, metabolic dysregulation, and increased cardiovascular risk [2]. The global demographic shift toward aging populations necessitates innovative therapeutic strategies addressing reproductive senescence beyond conventional hormone replacement therapy (HRT), which carries well-documented long-

term safety concerns including increased malignancy risk [3].

Ovarian aging is characterized by progressive follicular depletion, elevated follicle-stimulating hormone (FSH), and dysregulated inflammatory homeostasis [4]. At the cellular level, accumulation of senescent cells expressing senescence-associated β-galactosidase (SA-β-gal) and secreting pro-inflammatory senescence-associated secretory phenotype (SASP) factors drives tissue dysfunction [3,5]. The tumor suppressor p53 plays a pivotal role in orchestrating cellular senescence responses to accumulated DNA damage and oxidative stress [6,7]. Inflammatory dysregulation, characterized by elevated tumor necrosis factor-alpha (TNF-α) and decreased interleukin-10 (IL-10), further exacerbates the aging phenotype [8,9].

Mesenchymal stem cells (MSCs) have emerged as therapeutic candidates for regenerative medicine through their paracrine effects rather than direct differentiation [10-12]. Human umbilical cord-derived MSCs (HUMCMSCs) offer advantages over other MSC sources, including non-invasive procurement, higher proliferative capacity, and superior immunomodulatory properties [13-16]. Critically, the secretome of MSCs (S-MSCs), comprising growth factors, cytokines, extracellular vesicles, and microRNAs, replicates therapeutic effects while circumventing challenges associated with cellular therapies, including tumorigenicity, immune rejection, and regulatory complexity [17-19]. Previous investigations have demonstrated the efficacy of S-MSCs in various reproductive pathologies. Previous studies also reported the restoration of ovarian function in chemotherapy-induced ovarian insufficiency following S-MSC administration [20,21]. However, these studies primarily focused on acute models of chemically induced ovarian injury, which differ mechanistically from the gradual, multifactorial deterioration observed in natural aging. To our knowledge, this is the first investigation to systematically evaluate the therapeutic potential of human umbilical cord MSC-derived secretome (S-HUMCMSCs) in a naturally aged ovary model, directly benchmarked against standard hormone replacement therapy. However, a systematic evaluation of S-HUMCMSCs' effects on naturally aged ovaries, encompassing hormonal, inflammatory, senescence, and structural parameters, remains unexplored.

We hypothesized that S-HUMCMSCs would ameliorate multiple hallmarks of ovarian aging by coordinating the modulation of hormonal, inflammatory, and cellular senescence pathways. Using a validated murine natural aging model, we conducted a comprehensive assessment of the effects of S-HUMCMSCs on FSH levels, senescent cell burden, inflammatory markers (TNF-α and IL-10), p53 expression, and follicular morphology, comparing their efficacy with that of 17β-estradiol treatment.

Materials and methods

Animals

To ensure transparency and compliance with ARRIVE guidelines, animal allocation and sample inclusion/exclusion were documented throughout the study. Female BALB/c mice were obtained from SCCR Indonesia Laboratory and maintained under standard conditions (22 ± 2 °C, 55 ± 5% humidity, 12-hour light/dark cycle) with ad libitum access to standard chow and water. The study employed two age groups: young adults (4 months old, n = 6) and naturally aged (12 months old, n = 30). Aged mice were screened for irregular estrous cycles via daily vaginal cytology for 5 consecutive days. Only mice displaying prolonged or absent estrous cycles were included, confirming ovarian aging phenotype. Sample size calculation using Federer's formula [$(n-1)(t-1) \geq 15$, where t = number of groups] yielded n = 9 per group. To accommodate possible attrition or exclusion during screening, one additional mouse per group was included (n = 10 each), totaling 30 aged mice. Aged mice were randomly assigned to: (1) Vehicle control (PBS, n = 10); (2) 17β-estradiol (n = 10); (3) S-HUMCMSCs (n = 10). Young mice served as healthy controls (n = 6). Blinding was implemented at multiple levels: Investigators responsible for treatment administration were distinct from those conducting outcome assessments. Sample codes were anonymized during ELISA measurement, histological evaluation, and statistical analysis to ensure blinding to group identity. Data unblinding occurred only after all analyses were finalized. No animals were excluded after allocation due to death or handling issues. However, variability in endpoint detection led to differences in effective sample numbers for certain

assays. Specifically, P53 expression was quantifiable in only three young control ovaries (others were below the detection threshold), and TNF-α levels were undetectable in several healthy control samples. These instances were documented as n < group total in figure legends.

HUMCMSC isolation and culture

Human umbilical cords from healthy full-term deliveries were obtained following written informed consent from the mothers, in accordance with the Declaration of Helsinki and approved by the Institutional Ethics Committee of Faculty of Medicine Universitas Islam Sultan Agung, Semaramg (Approval No 116/IV/Komisi Bioetik/2025). Human umbilical cords from healthy full-term deliveries were obtained following informed consent. Cord tissue was washed extensively in PBS containing 1% penicillin-streptomycin, then Wharton's jelly was mechanically dissected and enzymatically digested with 0.1% collagenase type I (Worthington) for 2 h at 37 °C. Released cells were collected by centrifugation (300 g, 10 min), resuspended in complete medium (DMEM/F12 supplemented with 10% FBS, 1% penicillin-streptomycin), and plated in T75 flasks at 5×10^3 cells/cm². Cultures were maintained at 37 °C, 5% CO_2, with medium changes every 3 days. Upon reaching 80% - 90% confluence, cells were passaged using TrypLE Express. Passage 3 - 5 HUMCMSCs were used for secretome production [11,22-24].

HUMCMSC characterization

Flow cytometry was performed on passage 3 HUMCMSCs. Cells (2×10^6/mL) were incubated with fluorochrome-conjugated antibodies (CD90-FITC, CD29-PE, CD45-APC, CD31-PE) for 30 min at 4 °C, then analyzed on a BD FACSCelesta (BD Biosciences) with FlowJo software. For adipogenic differentiation, confluent cultures were treated with adipogenic medium (DMEM supplemented with 10% FBS, 1 μM dexamethasone, 0.5 mM isobutylmethylxanthine, 10 μg/mL insulin, 100 μM indomethacin) for 21 days. Lipid droplets were visualized with Oil Red O staining. Osteogenic differentiation employed osteogenic medium (DMEM supplemented with 10% FBS, 100 nM dexamethasone, 10 mM β-glycerophosphate, 50 μM ascorbic acid-2-phosphate) for 21 days. Calcium deposition was detected with Alizarin Red S staining [25,26].

Secretome production and processing

Passage 3 - 5 HUMCMSCs at 80% confluence were washed three times with PBS and cultured in serum-free DMEM/F12 under hypoxic conditions (5% O_2, 5% CO_2, 37 °C) for 24 h using a hypoxia chamber (Stemcell Technologies). Conditioned medium was collected, centrifuged (300 g, 10 min; then 2,000 g, 20 min) to remove cells and debris, and filtered through 0.22 μm membranes. A concentrated secretome was prepared using tangential flow filtration (Millipore) with 3 kDa molecular weight cutoff membranes, yielding proteins/factors with molecular weights between 3 and 750 kDa. Protein concentration was quantified by BCA assay (Pierce) and aliquots were stored at –80 °C. Secretome batches were validated for consistency via protein profiling and bioactivity assays [26,27]. To evaluate the bioactive component content, cytokine and growth factor levels in the secretome were quantified using enzyme-linked immunosorbent assay (ELISA) kits specific for interleukin-10 (IL-10), vascular endothelial growth factor (VEGF), and stromal cell-derived factor-1 (SDF-1). Secretome batches were validated for consistency through protein profiling and bioactivity assays.

Experimental design and treatment regimen

Following baseline assessments (Day 1 - 7) and validation of aging phenotype (Day 8 - 13), mice received interventions on Days 14 and 16 via tail vein injection (200 μL volume):

1) S-HUMCMSCs group: 250 μg total protein in PBS (125 μg per injection)

2) 17β-estradiol group: 3 μg/kg (stock prepared as 1 mg estradiol in 500 μL DMSO, diluted 1:100 in saline)

3) Vehicle control: PBS

4) Young control: No treatment

Mice were euthanized on Day 21 (5 days post-second injection) under isoflurane anesthesia followed by cervical dislocation. Blood was collected via cardiac puncture, allowed to clot (30 min, room temperature), and centrifuged (1,000 g, 15 min) to obtain serum. Ovaries were dissected; one ovary was immediately snap-frozen in liquid nitrogen for molecular analyses,

while the contralateral ovary was fixed in 4% paraformaldehyde for histology.

Serum hormone and cytokine measurements

FSH, TNF-α, IL-10, and p53 were quantified in serum using species-specific sandwich ELISA kits (Elabscience) per manufacturer protocols. Briefly, 100μL serum samples or standards were incubated in antibody-coated microplates (1 h, room temperature), washed five times, incubated with HRP-conjugated detection antibody (1 h, 37 °C), washed again, developed with TMB substrate (10 min, 37 °C), stopped with sulfuric acid, and read at 450 nm (BioTek Synergy H1). Standard curves were generated using four-parameter logistic fitting. All samples were analyzed in duplicate with intra-assay CV < 10%.

Senescence-associated β-Galactosidase staining

Frozen ovarian tissue sections (10 μm) were fixed in 0.2% glutaraldehyde/2% formaldehyde (5 min, room temperature), washed with PBS, and incubated overnight (37 °C) in X-gal staining solution (1mg/mL X-gal, 5 mM potassium ferrocyanide, 5 mM potassium ferricyanide, 2 mM $MgCl_2$, 150 mM NaCl in citric acid/phosphate buffer pH 6.0). After washing, sections were counterstained with nuclear fast red, dehydrated, and mounted. SA-β-gal-positive cells (blue cytoplasmic staining) were quantified using ImageJ software. Five random fields per section (400× magnification) were captured, thresholded for blue chromogen, and analyzed using the "Analyze Particles" function. Results are expressed as percentage of positively stained cells relative to total cells (nuclear fast red-positive nuclei).

Histological analysis

Paraformaldehyde-fixed ovaries were paraffin-embedded, sectioned (5 μm), and stained with hematoxylin and eosin following standard protocols. Every 9th section was analyzed to avoid counting the same follicle twice. Follicles were classified according to established criteria, primordial when the oocyte was surrounded by a single layer of flattened granulosa cells. The primary oocyte is surrounded by a single layer of cuboidal granulosa cells. Secondary is multiple layers (≥ 2) of granulosa cells without a visible antrum, and antral is a fluid-filled antral space. Follicle counts were performed on five randomly selected sections per ovary by two independent blinded observers using a Nikon Eclipse Ni-U microscope (200× magnification). Only follicles with a visible oocyte nucleus were counted to prevent duplicate counting. Results represent the mean follicle number per section.

Quantification and statistical analysis

All data are presented as mean ± standard deviation (SD) unless otherwise noted. Sample sizes are indicated in figure legends. Statistical analyses were performed using SPSS Statistics version 26.0. Data distribution was assessed using the Shapiro-Wilk test. Homogeneity of variance was evaluated with Levene's test. For normally distributed data with homogeneous variance, one-way ANOVA followed by the Tukey test was employed. Non-normally distributed data were analyzed using the Kruskal-Wallis test followed by the Mann-Whitney U test with Bonferroni correction for multiple comparisons. Pre-post comparisons within groups (FSH levels) utilized a paired t-test (normal distribution) or a Wilcoxon signed-rank test (non-normal distribution). Statistical significance was defined as $p < 0.05$ (one-tailed). Specific statistical tests for each dataset are noted in the figure legends. No outliers were excluded. Investigators were blinded to treatment groups during data acquisition and analysis, where applicable (histology, senescence quantification).

Ethical approval

All experimental procedures were approved by the Ethics Committee of Sultan Agung Islamic University Faculty of Medicine (Protocol No.116/IV/Komisi Bioetik/2025) and conducted according to ARRIVE guidelines.

Results and discussion

Our investigation provides comprehensive evidence that the administration of S-HUMCMSCs ameliorates multiple dimensions of ovarian aging through coordinated effects on hormonal regulation, inflammatory homeostasis, cellular senescence, and tissue architecture. These findings advance understanding of MSC secretome mechanisms while establishing practical therapeutic potential. The observed TNF-α reduction (a 97.6% decrease from the aged baseline) and IL-10 elevation following S-HUMCMSCs treatment demonstrate a potent immunomodulatory capacity. This anti-inflammatory

effect likely stems from multiple secretome components, including IL-10 itself, transforming growth factor-β (TGF-β), and prostaglandin E2, which collectively polarize macrophages from M1 (pro-inflammatory) toward M2 (anti-inflammatory) phenotypes [20]. Additionally, growth factors such as hepatocyte growth factor (HGF) and vascular endothelial growth factor (VEGF) within S-HUMCMSCs activate the PI3K/AKT and MAPK/ERK pathways, suppressing NF-κB-mediated transcription of pro-inflammatory cytokines [28,29].

The FSH reduction following S-HUMCMSCs treatment suggests restored hypothalamic-pituitary-ovarian axis function. This may result from improved ovarian follicular competence, thereby strengthening negative feedback through estradiol and inhibin secretion. Alternatively, S-HUMCMSCs-derived microRNAs (miR-21, miR-146a) may directly modulate the expression of steroidogenic enzymes, particularly aromatase (CYP19A1), thereby enhancing local estrogen production [30]. The insulin-like growth factor-1 (IGF-1) in S-HUMCMSCs may increase granulosa cell FSH sensitivity via PI3K/AKT activation, thereby reducing the required circulating FSH levels [31].

S-HUMCMSCs characterization and validation

Isolated HUMCMSCs exhibited characteristic spindle-like morphology and plastic adherence (**Figure 1(A)**). Tri-lineage differentiation capacity was demonstrated through Oil Red O-positive adipogenic differentiation (**Figure 1(B)**) and Alizarin Red S-positive osteogenic differentiation (**Figure 1(C)**), fulfilling International Society for Cellular Therapy criteria. Flow cytometry confirmed MSC identity: CD90 (97.60%), CD29 (97.70%), with minimal CD45 (1.50%) and CD31 (3.20%) expression (**Figure 1(D)**). Secretome profiling revealed the presence of key cytokines and growth factors, including interleukin-10 (IL-10), vascular endothelial growth factor (VEGF), and stromal cell-derived factor-1 (SDF-1). The average concentrations (mean ± SD, pg/mL) from three secretome batches were 21.21 ± 9.45 for IL-10, 408.93 ± 22.82 for VEGF, and 569.18 ± 77.29 for SDF-1 (**Figure 1(E)**), indicating stable cytokine and growth factor production across preparations.

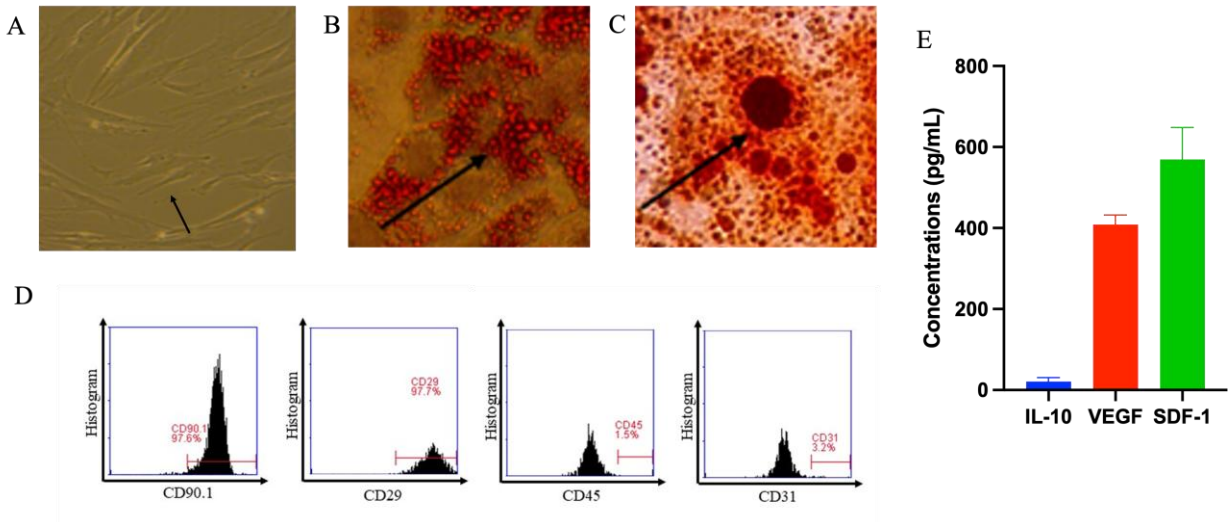

Figure 1 Characterization of Human Umbilical Cord-Derived Mesenchymal Stem Cells (A) Phase-contrast microscopy showing characteristic spindle-like morphology of cultured HUMCMSCs (passage 3). Scale bar: 100 μm. (B) Oil Red O staining demonstrates adipogenic differentiation capacity with accumulated lipid droplets. Scale bar: 50 μm. (C) Alizarin Red S staining showing calcium deposition, indicating osteogenic differentiation capacity. Scale bar: 50 μm. (D) Flow cytometry analysis showing expression of positive MSC markers (CD90: 97.60%, CD29: 97.70%) and absence of hematopoietic/endothelial markers (CD45: 1.50%, CD31: 3.20%). (E) Cytokine and growth factor concentration on secretome analyses under ELISA assay, n = 3.

Validation of the ovarian aging model

To establish a physiologically relevant model, we employed naturally aged 12-month-old female BALB/c mice. Histological examination revealed significant follicular depletion across developmental stages. Secondary follicle counts decreased from 1.8 ± 0.2 in young (4-month) controls to 0.2 ± 0.1 in aged mice ($p < 0.05$). Primary follicles similarly declined from 1.8 ± 0.2 to 0.1 ± 0.05 ($p < 0.05$) (**Figures 2(A) - 2(E)**). Antral and primordial follicles showed numerical but non-significant reductions. Critically, serum FSH levels increased 2.5-fold in aged mice (5.5 ± 0.4 vs 2.2 ± 0.1 mIU/mL, $p < 0.001$) (**Figure 2(F)**), confirming disrupted hypothalamic-pituitary-ovarian axis function characteristic of reproductive aging.

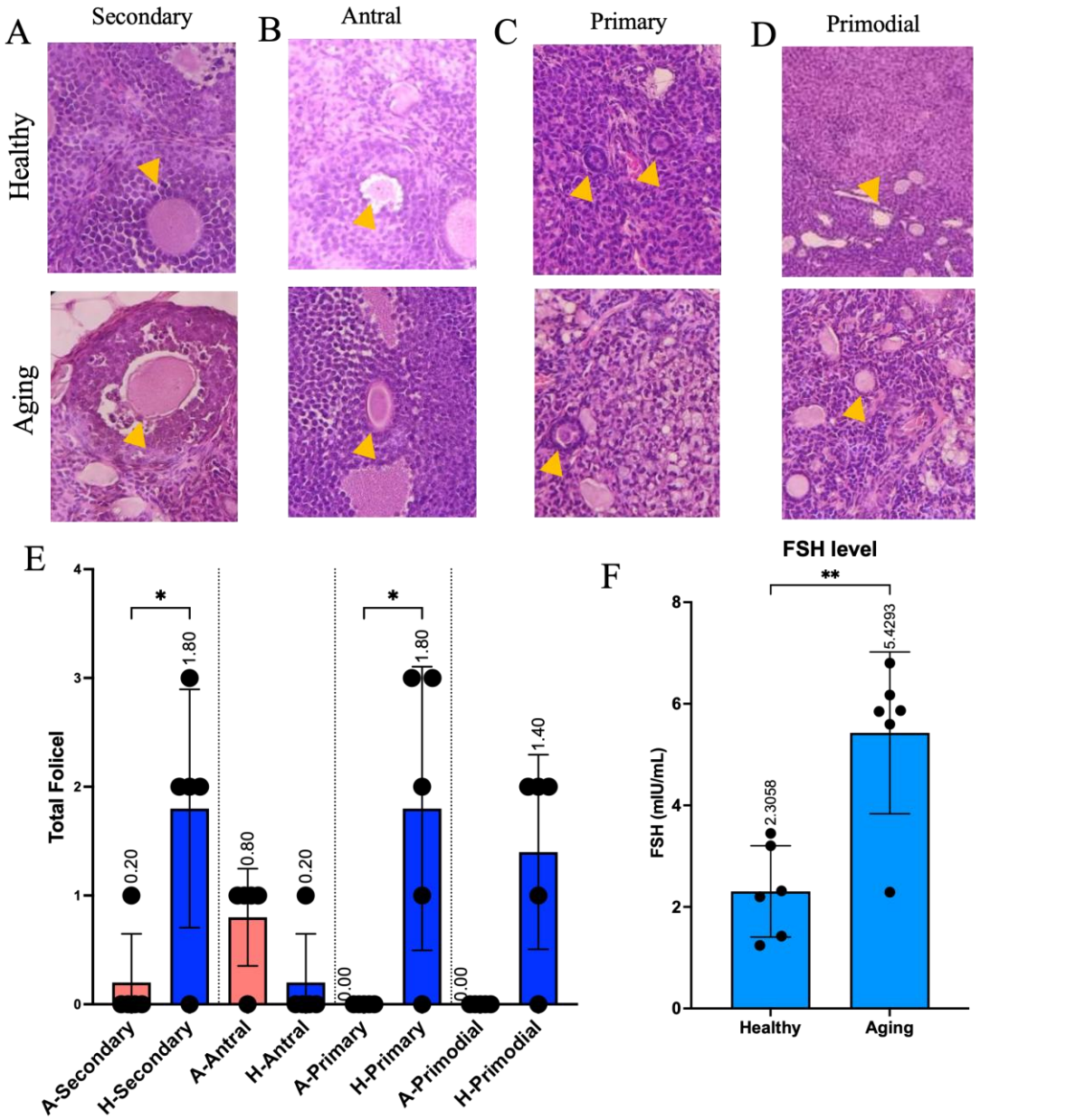

Figure 2 Validation of Natural Ovarian Aging Model (A - D) Representative histological images (H&E staining) of ovarian sections from young (4-month) and aged (12-month) mice showing follicles at different developmental stages. Yellow arrows indicate primordial, primary, secondary, and antral follicles. Scale bar: 100 µm. (E) Quantification of follicle numbers across developmental stages. Data shown as mean ± SEM (n = 3 per group). *$p < 0.05$ vs. young controls (Student's t-test). (F) Serum FSH levels in young and aged mice are significantly elevated with aging. Data shown as mean ± SEM (n = 6 per group). **$p < 0.001$ vs. young controls (Student's t-test).

S-HUMCMSCs reduce systemic inflammatory burden

Aged control mice exhibited profound inflammatory activation with TNF-α levels reaching 188.23 ± 83.31 ng/mL compared to 1.26 ± 1.45 ng/mL in young controls ($p < 0.001$). S-HUMCMSC treatment dramatically reduced TNF-α levels to 4.55 ± 4.78 ng/mL, comparable to the 17β-estradiol group (8.24 ± 11.36 ng/mL) and not significantly different from young controls ($p = 0.942$) (**Figure 3(A)**). Post-hoc analysis confirmed S-HUMCMSCs and estradiol treatments did not differ significantly ($p > 0.05$), while both differed markedly from aged controls ($p < 0.001$).

The anti-inflammatory capacity was assessed by quantifying IL-10. Aged controls showed reduced IL-10 (1.73 ± 1.22 ng/mL) relative to baseline. S-HUMCMSCs administration elevated IL-10 to 7.55 ± 7.77 ng/mL, significantly exceeding young controls (1.06 ± 1.17 ng/mL, $p = 0.019$) and aged controls ($p = 0.033$) (**Figure 3(B)**). This response exceeded that of 17β-estradiol treatment (5.85 ± 5.58 ng/mL), although the differences were not statistically significant ($p = 0.515$).

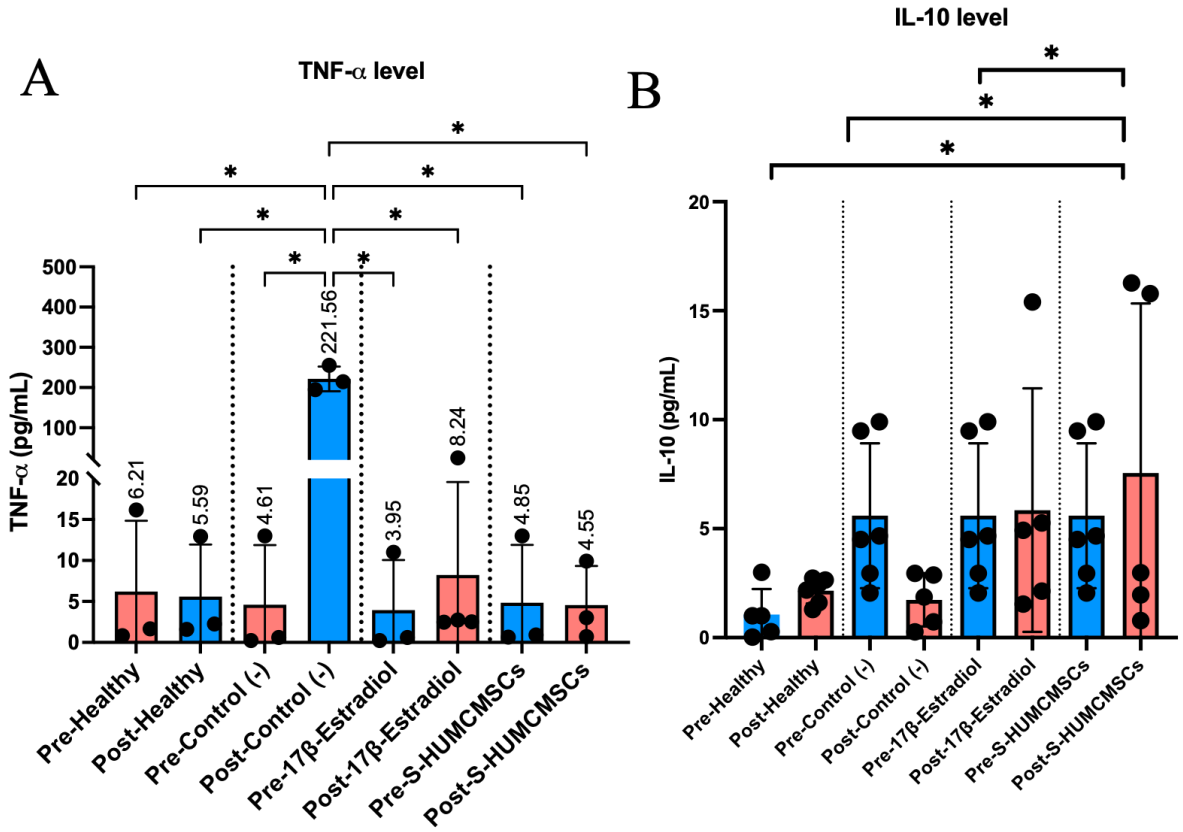

Figure 3 S-HUMCMSCs Reduce Systemic Inflammation (A) Serum TNF-α concentrations across experimental groups. Data shown as mean ± SD (n = 5 - 6 per group). ****$p < 0.0001$ vs. indicated groups (one-way ANOVA with Turkey's test). (B) Serum IL-10 concentrations across experimental groups. Data shown as mean ± SD (n = 6 per group). *$p < 0.05$ vs. indicated groups (one-way ANOVA with Turkey's test).

Hormonal axis restoration

FSH elevation represents a cardinal biomarker of reproductive aging. Aged controls demonstrated sustained FSH elevation (5.43 ± 1.59 mIU/mL) compared to young mice (1.10 ± 0.03 mIU/mL, $p = 0.017$). S-HUMCMSCs reduced FSH to 3.07 ± 2.69 mIU/mL, not significantly different from young controls ($p = 0.878$) or 17β-estradiol treatment (4.01 ± 1.50 mIU/mL, $p = 1.000$) (**Figure 4**). These data indicate partial restoration of hypothalamic-pituitary sensitivity and/or improved ovarian follicular function.

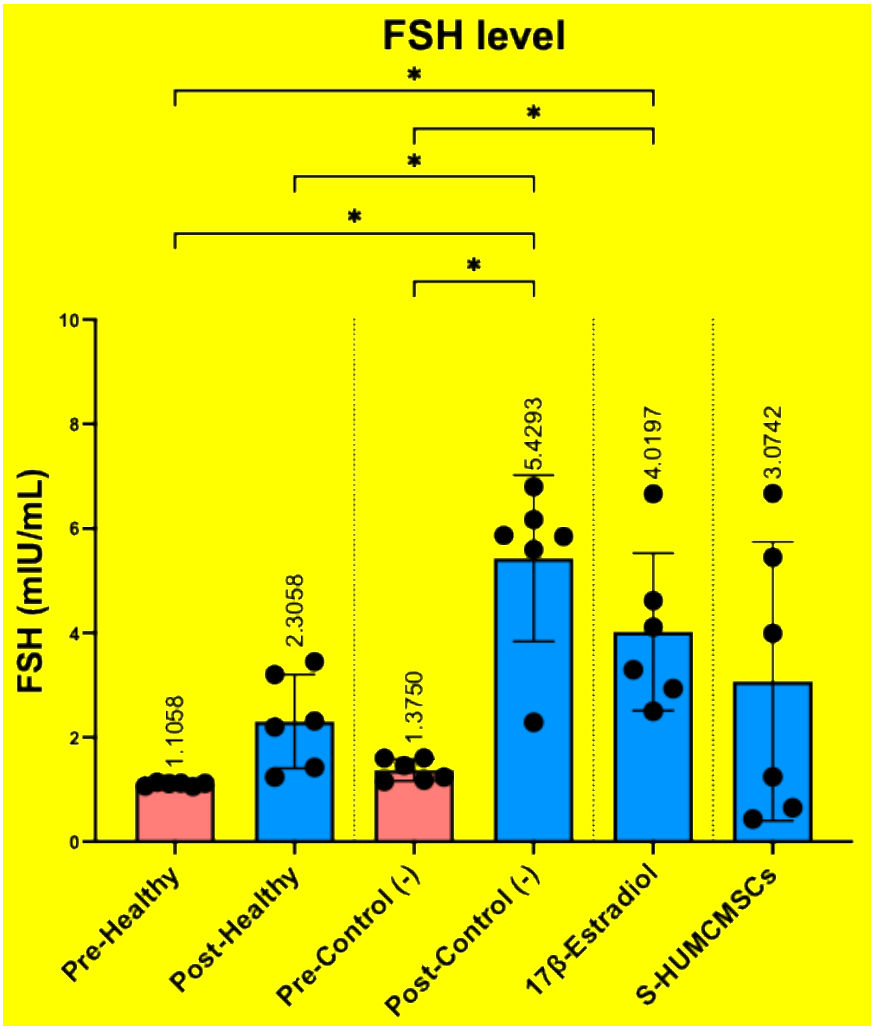

Figure 4 S-HUMCMSCs restore Hormonal Homeostasis. Serum FSH levels across experimental groups. Pre-treatment values are shown for young and aged mice. Post-treatment values are shown for all groups following a 21-day intervention period. Data shown as mean ± SD (n = 6 per group). *$p < 0.05$ vs. indicated groups (one-way ANOVA with Turkey's test).

Attenuation of cellular senescence

Senescent cell accumulation, quantified via SA-β-gal activity, increased dramatically with aging (27.35 ± 0.82% in aged controls vs 6.95 ± 0.49% in young mice, $p < 0.001$). S-HUMCMSCs treatment reduced senescent cell burden to 8.37 ± 0.85%, significantly lower than 17β-estradiol treatment (18.75 ± 0.76%, $p < 0.001$) and approaching young control levels ($p = 0.004$) (**Figures 5(A) – (B)**). This superior efficacy suggests S-HUMCMSCs engage senescence-attenuating or senostatic mechanisms beyond hormonal modulation.

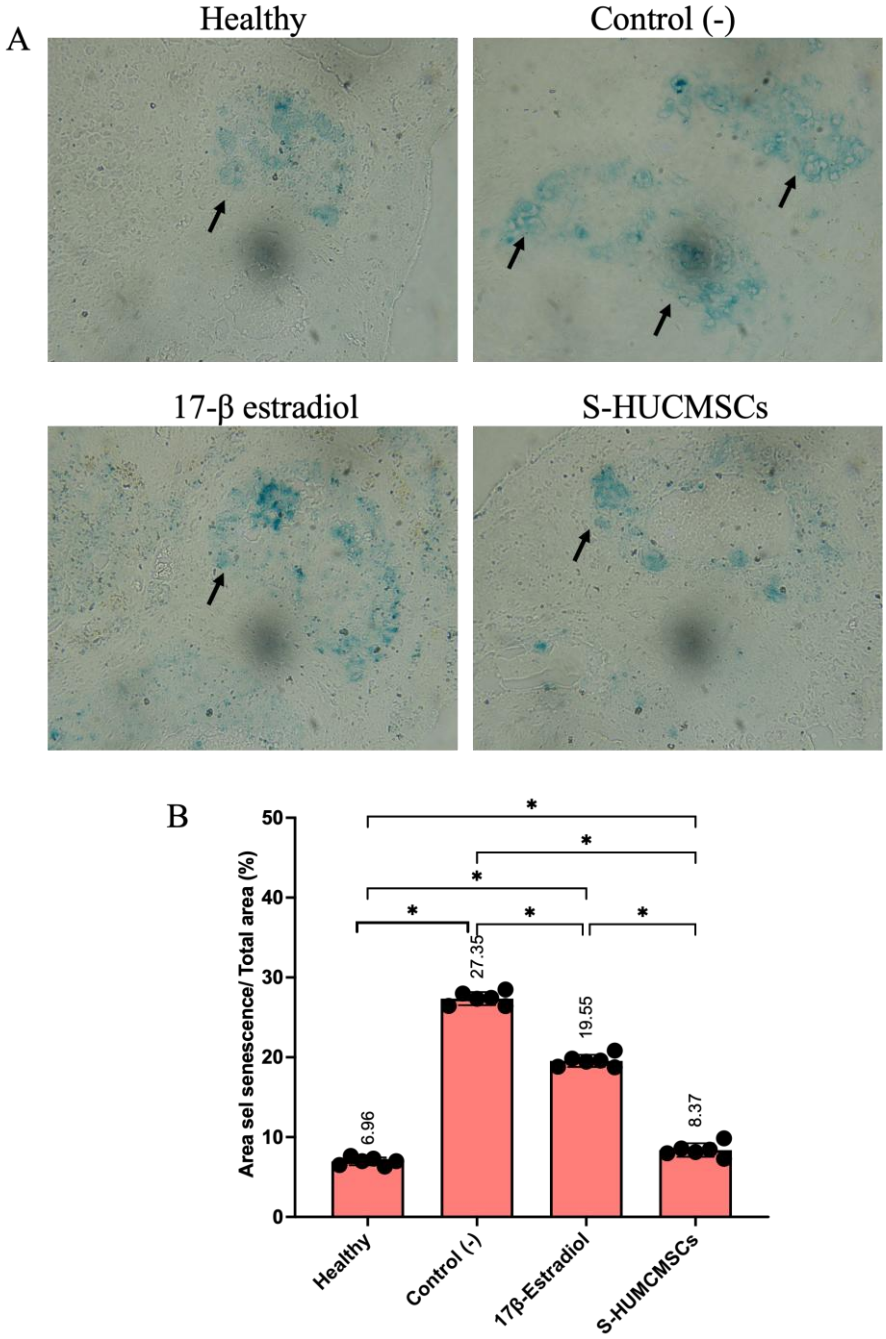

Figure 5 S-HUMCMSCs Attenuates Cellular Senescence (A) Representative images of SA-β-gal staining (blue) in ovarian tissue sections from each experimental group. Blue cytoplasmic staining indicates senescent cells. Scale bar: 50 μm. (B) Quantification of senescent cell percentage across groups. Data shown as mean ± SD (n = 6 per group). ****$p <$ 0.0001 vs. indicated groups (one-way ANOVA with Turkey's test). Five random fields per section were analyzed.

Molecular assessment of senescence pathways revealed p53 protein elevation in aged controls (549.67 ± 243.62 arbitrary units) versus young mice (34.80 ± 16.88, p = 0.007). S-HUMCMSCs decreased p53 expression to 179.17 ± 170.48, significantly lower than aged controls (p = 0.025) and not different from young mice (p = 0.426) (**Figure 6**). In contrast, 17β-estradiol treatment yielded intermediate p53 levels (401.43 ± 288.64), differing from young controls (p = 0.040) but not from aged controls (p = 0.284) or S-HUMCMSCs (p = 0.157).

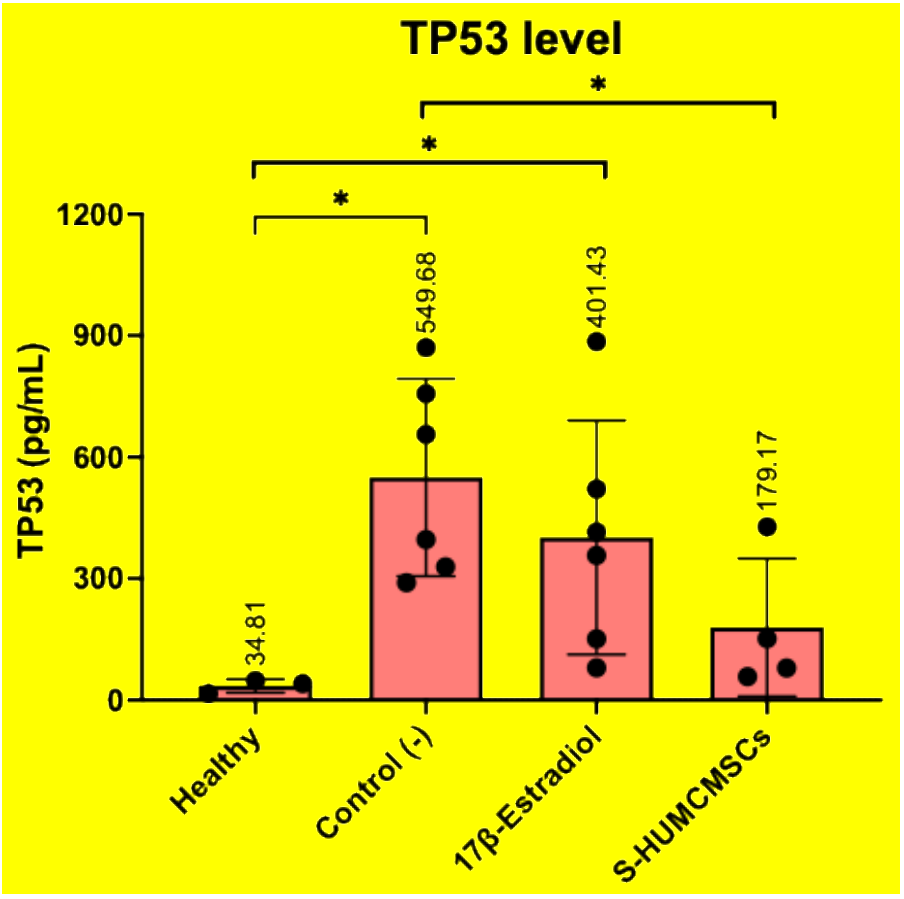

Figure 6 S-HUMCMSCs Reduce p53 Expression. Serum p53 protein levels were measured by ELISA across experimental groups. Data shown as mean ± SD (n = 3 - 6 per group). *$p < 0.05$, **$p < 0.01$ vs. indicated groups (one-way ANOVA with Turkey's test).

Preservation of follicular architecture

Histomorphometric analysis revealed differential effects across follicular stages, with follicle counts per ovary determined by systematic sampling of serial sections (**Figures 7(A) - (D)**). Primordial follicles showed non-significant trends across groups, whereas antral, primary, and secondary follicles exhibited patterns consistent with partial preservation of the growing follicle pool in treated mice, although the study was not specifically powered to detect small differences in follicle number between groups. S-HUMCMSC-treated ovaries maintained follicular counts comparable to young controls, but these differences did not reach statistical significance in this cohort (**Figures 7(A) - (D)**). Atretic follicles were defined as those showing disrupted or collapsed granulosa cell layers, detachment from the basement membrane, oocyte degeneration or nuclear pyknosis, and/or multiple pyknotic granulosa nuclei within the largest follicle cross-section.

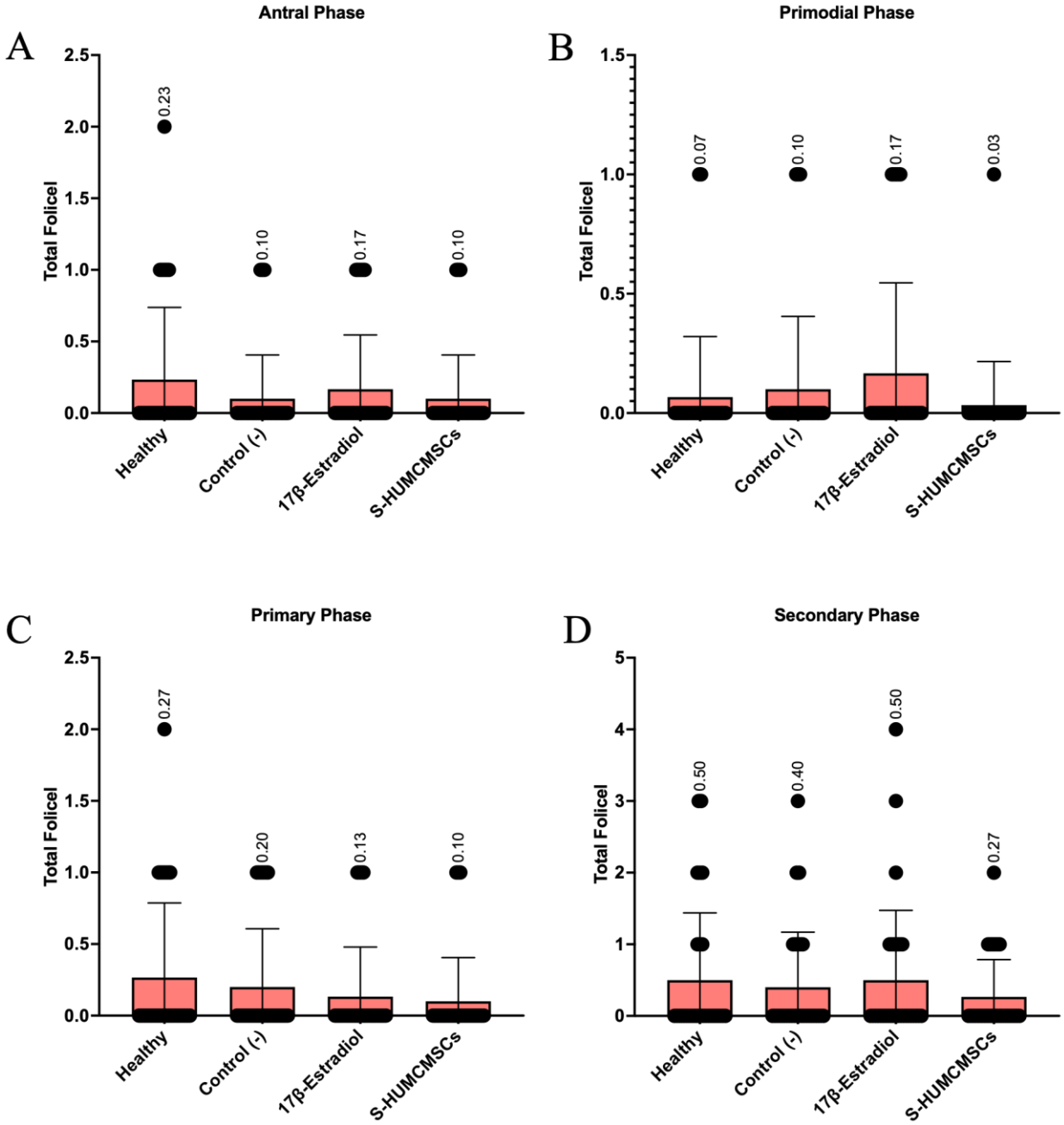

Figure 7 Effects of S-HUMCMSCs on Ovarian Follicular Architecture (A - D) Quantification of follicle numbers at different developmental stages: Antral (A), primordial (B), primary (C), and secondary (D) follicles. Data shown as mean ± SD (n = 6 per group). Statistical analysis performed using one-way ANOVA; specific p-values are indicated where significant differences were observed.

S-HUMCMSCs demonstrated superior efficacy over 17β-estradiol in reducing senescent cell burden (69% vs 31% reduction). This advantage likely reflects multi-factorial mechanisms absent from pure hormonal intervention. S-HUMCMSCs deliver antioxidant enzymes, including superoxide dismutase, catalase, and glutathione peroxidase, that neutralize reactive oxygen species, driving DNA damage and p53 activation [32,33]. Growth factors (PDGF, FGF) activate survival pathways (PI3K/AKT/mTOR) that antagonize p53-mediated pro-apoptotic signaling [34,35]. Exosomal cargo, including anti-senescence microRNAs (miR-34a, miR-146a), directly modulates p53/p21 signaling cascades [36,37]. The reduction in p53 observed with S-

HUMCMSCs treatment (a 67% decrease) provides molecular evidence for attenuated DNA damage responses and cell cycle arrest. While 17β-estradiol also reduced p53, the effect was less pronounced (27%), suggesting that hormonal effects primarily address downstream consequences rather than the root causes of cellular stress.

Conventional 17β-estradiol therapy operates through estrogen receptor (ER) activation, predominantly ERα in the hypothalamus/pituitary and reproductive tissues. This induces transcriptional programs that support proliferation, vasodilation, and lipid metabolism, while suppressing certain inflammatory pathways through ER-NF-κB interactions [38,39]. However, sustained ERα activation carries oncogenic risks through hyperproliferation and genotoxic metabolite (4-hydroxyestradiol) generation [40,41]. In contrast, the observed benefits of S-HUMCMSCs appear to arise through hormone-independent mechanisms, such as paracrine immunomodulation, antioxidant delivery, pro-regenerative signaling, and microRNA-mediated regulation, which may theoretically reduce such estrogen receptor-related risks. Nevertheless, dedicated toxicological and long-term safety evaluations are required before establishing any comparative safety advantage. This cell-free approach avoids tumorigenicity concerns associated with cellular therapies while maintaining biological complexity absent from single-molecule pharmaceuticals. The comparable efficacy to estradiol in reducing FSH, combined with superior senescence control and inflammation resolution, positions S-HUMCMSCs as a potentially safer long-term intervention.

This study presents certain limitations that warrant consideration. The assessment at a single post-treatment time point (21 days) limits conclusions about the durability of the observed effects; thus, longitudinal evaluations are required to determine the persistence of benefits and optimal retreatment intervals. Although multiple outcome parameters were analyzed, the underlying mechanisms remain to be elucidated through targeted gain- and loss-of-function approaches that address specific components of the secretome. Moreover, despite its physiological relevance, the murine natural aging model does not fully recapitulate the temporal progression and hormonal dynamics of human perimenopause, highlighting the need for validation in non-human primate models. The absence of a comprehensive toxicological assessment also limits immediate translational applicability. Finally, the relatively modest sample size in follicular morphometry analyses may have reduced the statistical power to detect subtle preservation effects.

Conclusions

In conclusion, S-HUMCMSCs showed amelioration of multiple hallmarks of ovarian aging in naturally aged mice, including normalization of FSH levels, marked attenuation of systemic inflammation (TNF-α/IL-10), reduction of senescent cell burden and p53 expression, and qualitative preservation of follicular architecture relative to aged controls and 17β-estradiol. These findings support a hormone-independent, paracrine mechanism by which the secretome modulates hypothalamic-pituitary-ovarian axis function, inflammatory homeostasis, and cellular senescence pathways in the context of reproductive aging. In addition, interpretation of these results is constrained by the single 21-day observation time point, modest sample sizes, particularly for follicular morphometry, and the absence of comprehensive toxicological and mechanistic (gain-/loss-of-function) studies. Future investigations should therefore incorporate longitudinal designs to define the durability and optimal scheduling of S-HUMCMSC administration, systematically dissect the contribution of specific secretome components and perform detailed safety and efficacy assessments in higher-order preclinical models that more closely recapitulate human perimenopausal physiology.

Acknowledgements

We would like to express our gratitude to everyone who supported this study.

Declaration of generative AI in scientific writing

The author utilized artificial intelligence tools solely for grammar and language editing purposes to enhance readability, as the author is not a native English speaker. The AI was not used for data analysis, interpretation, or content generation. The author takes full responsibility for the accuracy, integrity, and originality of all content presented in the manuscript.

CRediT author statement

Yulice Soraya Nur Intan, Dono Indarto, Soetrisno: Conceptualization; Methodology; Software. **Abdurahman Laqif**: Data curation; Writing - Original draft preparation. **Yulice Soraya Nur Intan, Dono Indarto**: Visualization; Investigation. **Paramasari Dirgahayu**: Supervision. **Soetrisno**: Software; Validation. **Paramasari Dirgahayu, Dono Indarto**: Writing - Reviewing and Editing.

References

[1] K Shirasuna and H Iwata. Effect of aging on the female reproductive function. *Contraception and Reproductive Medicine* 2017; **2**, 23.

[2] R Costa, TP Tuomainen, J Virtanen, L Niskanen and E Bertone-Johnson. Associations of reproductive factors with postmenopausal follicle stimulating hormone. *Women's Midlife Health* 2022; **8**, 8.

[3] JVV Isola, JD Hense, CAP Osório, S Biswas, J Alberola-Ila, SR Ocañas, A Schneider and MB Stout. Reproductive ageing: Inflammation, immune cells, and cellular senescence in the aging ovary. *Reproduction* 2024; **168(2)**, 230499.

[4] M Dean, BT Murphy and JE Burdette. Phytosteroids beyond estrogens: Regulators of reproductive and endocrine function in natural products. *Molecular and Cellular Endocrinology* 2017; **442**, 98-105.

[5] J Zhao, D Li, H Tang and L Tang. Association of vascular endothelial growth factor polymorphisms with polycystic ovarian syndrome risk: A meta-analysis. *Reproductive Biology and Endocrinology* 2020; **18**, 18.

[6] AL Fitzgerald, AA Osman, TX Xie, A Patel, H Skinner, V Sandulache and JN Myers. Reactive oxygen species and p21Waf1/Cip1 are both essential for p53-mediated senescence of head and neck cancer cells. *Cell Death & Disease* 2015; **6**, 1678.

[7] Q Chen, X Sun, X Luo, J Wang, J Hu and Y Feng. PIK3R3 inhibits cell senescence through p53/p21 signaling. *Cell Death & Disease* 2020; **11**, 798.

[8] R Rajah, B Valentinis and P Cohen. Insulin-like growth factor (IGF)-binding protein-3 induces apoptosis and mediates the effects of transforming growth factor-β1 on programmed cell death through a p53- and IGF-independent mechanism. *Journal of Biological Chemistry* 1997; **272(18)**, 12181-12188.

[9] JD Amaral, JM Xavier, CJ Steer and CMP Rodrigues. Targeting the p53 Pathway of Apoptosis. *Current Pharmaceutical Design* 2010; **16**, 2493-2503.

[10] YW Prajoko, A Putra, BT Dirja, AM Muhar and ND Amalina. The Ameliorating effects of MSCs in controlling Treg-mediated B-Cell depletion by Indoleamine 2, 3-dioxygenase induction in PBMC of SLE patients. *Open Access Macedonian Journal of Medical Sciences* 2022; **10**, 6-11.

[11] L Restimulia, S Ilyas, D Munir, A Putra, T Madiadipoera, F Farhat, RJ Sembiring, M Ichwan, ND Amalina and I Alif. The CD4+CD25+FoxP3+ Regulatory T cells regulated by MSCs suppress plasma cells in a mouse model of allergic rhinitis. *Medical Archives* 2021; **75(4)**, 256-261.

[12] MHB Kusumo, SA Husain and ND Amalina. Secretome MSCs restore α-Smooth muscle actin protein tissue expression in croton oil-induced hemorrhoid rats. 2023; **2(4)**, 138-146.

[13] BT Dirja, EH Wardoyo, A Putra and ND Amalina. Enhanced third degree burn wound healing by hypoxic mesenchymal stem cells' secretome: IL-10 upregulation and TNF-α/PGE2 suppression. *Trends in Sciences* 2024; **21(10)**, 8288.

[14] MM Hartanto, YW Prajoko, A Putra and ND Amalina. The combination of mesenchymal stem cells and bovine colostrum in reducing α-SMA expression and NLR levels in wistar rats after 50% fibrotic liver resection. *Open Access Macedonian Journal of Medical Sciences* 2022; **10**, 1634-1639.

[15] D Munir, IP Nasution, L Restimulia, A Putra and ND Amalina. The role of mesenchymal stem cells in allergic rhinitis and its relationship with IL-10, plasma cells and regulatory T cells. *Medicinski Glasnik* 2023; **20(2)**, 175-180.

[16] NF Hamra, A Putra, A Tjipta5, ND Amalina and T Nasihun. Hypoxia mesenchymal stem cells accelerate wound closure improvement by controlling α-smooth muscle actin expression in the full-thickness animal model. *Open Access Macedonian Journal of Medical Sciences* 2021; **8**, 35-41.

[17] S Bartaula-Brevik, AI Bolstad, K Mustafa and TO Pedersen. Secretome of mesenchymal stem cells grown in hypoxia accelerates wound healing and vessel formation *in vitro*. *International Journal of Stem Cell Research & Therapy* 2017; **4(1)**, 045.

[18] Q Zhao, K Larios, Y Naaldijk, LS Sherman, A Chemerinski, K Okereke, P Rameshwar, A Lemenze, NC Douglas and SS Morelli. Mesenchymal stem cell secretome alters gene expression and upregulates motility of human endometrial stromal cells. *Reproduction* 2023; **166(2)**, 161-174.

[19] TO Ribeiro, BM Silveira, MC Meira, ACO Carreira, MC Sogayar, R Meyer and V Fortuna. Investigating the potential of the secretome of mesenchymal stem cells derived from sickle cell disease patients. *PLoS One* 2019; **14(10)**, 0222093.

[20] RM Chugh, H Park, S Esfandyari, A Elsharoud, M Ulin and A Al-Hendy. Mesenchymal stem cell-conditioned media regulate steroidogenesis and inhibit androgen secretion in a PCOS cell model via BMP-2. *International Journal of Molecular Sciences* 2021; **22(17)**, 9184.

[21] H Wang, X Feng, T Wang, J Pan, Z Zheng, Y Su, H Weng, L Zhang, L Chen, L Zhou and L Zheng. Role and mechanism of the p-JAK2/p-STAT3 signaling pathway in follicular development in PCOS rats. *General and Comparative Endocrinology* 2023; **330**, 114138.

[22] YI Mayasari, P Subchan, A Putra, C Chodijah, A Hussana, T Sumarawati, ND Amalina and RCS Irawan. Secretome hypoxia mesenchymal stem cells inhibited ultraviolet radiation by inhibiting interleukin-6 through nuclear factor-kappa beta pathway in hyperpigmentation animal models. *Open Access Macedonian Journal of Medical Sciences* 2023; **11**, 188-194.

[23] Z Zukhiroh, A Putra, C Chodidjah, T Sumarawati, P Subchan, S Trisnadi, N Hidayah and ND Amalina. Effect of secretome-hypoxia mesenchymal stem cells on regulating SOD and MMP-1 mRNA expressions in skin hyperpigmentation rats. *Open Access Macedonian Journal of Medical Sciences* 2022; **10**, 1-7.

[24] M Fredianto, H Herman, YD Ismiarto, A Putra, I Alif, ND Amalina and MA Nazar. Secretome of hypoxia-preconditioned mesenchymal stem cells enhance the expression of HIF-1a and bFGF in a rotator cuff tear model. *Medicinski Glasnik* 2023; **20(2)**, 242-248.

[25] AM Muhar, F Makharim, D Hermansyah, A Putra, N Hidayah, ND Amalina and I Alif. Hypoxic mesenchymal stem cell-conditioned medium accelerates wound healing by regulating IL-10 and TGF-β levels in a full-thickness-wound rat model. *Indonesian Journal of Biotechnology* 2022; **27(4)**, 187-194.

[26] J Angelina, A Putra, S Trisnadi, D Hermansyah, E Setiawan, T Sumarawati and ND Amalina. Hypoxia-conditioned mesenchymal stem cells (MSC) exosomes attenuate ultraviolet-B (UVB)-mediated malondialdehyde (MDA) and matrix metalloproteinase-1 (MMP-1) upregulation in collagen loss models. *Medicinski Glasnik* 2025; **22(1)**, 9-14.

[27] P Drawina, A Putra, T Nasihun, YW Prajoko, BT Dirja and ND Amalina. Increased serial levels of platelet-derived growth factor using hypoxic mesenchymal stem cell-conditioned medium to promote closure acceler- ation in a full-thickness wound. *Indonesian Journal of Biotechnology* 2022; **27(1)**, 36-42.

[28] FT Zohora, M Aliyu and AA Saboor-Yaraghi. Secretome-based acellular therapy of bone marrow-derived mesenchymal stem cells in degenerative and immunological disorders: A narrative review. *Heliyon* 2023; **9(7)**, 18120.

[29] RM Chugh, H Park, AE Andaloussi, A Elsharoud, S Esfandyari, M Ulin, L Bakir, A Aboalsoud, M Ali, D Ashour, P Igboeli, N Ismail, J McAllister and A Al-Hendy. Mesenchymal stem cell therapy ameliorates metabolic dysfunction and restores fertility in a PCOS mouse model through interleukin-10. *Stem Cell Research & Therapy* 2021; **12**, 388.

[30] FZ Stanczyk, SA Winer, JM Foidart and DF Archer. Comparison of estrogenic components used for hormonal contraception. *Contraception* 2024; **130**, 110310.

[31] EA Ariazi and VC Jordan. Estrogen-related receptors as emerging targets in cancer and metabolic disorders. *Current Topics in Medicinal Chemistry* 2006; **6(3)**, 203-215.

[32] S Wang, EA Konorev, S Kotamraju, J Joseph, S Kalivendi and B Kalyanaraman. Doxorubicin induces apoptosis in normal and tumor cells via distinctly different mechanisms: Intermediacy of H2O2- and p53-dependent pathways. *Journal of Biological Chemistry* 2004; **279(24)**, 25535-25543.

[33] W Xue, L Zender, C Miething, RA Dickins, E Hernando, V Krizhanovsky, C Cordon-Cardo and SW Lowe. Senescence and tumour clearance is triggered by p53 restoration in murine liver carcinomas. *Nature* 2007; **445**, 656-660.

[34] V Reyhani, M Tsioumpekou, T van Wieringen, L Rask, J Lennartsson and K Rubin. PDGF-BB enhances collagen gel contraction through a PI3K-PLCγ-PKC-cofilin pathway. *Scientific Reports* 2017; **7**, 8924.

[35] A Makker, MM Goel, V Das and A Agarwal. PI3K-Akt-mTOR and MAPK signaling pathways in polycystic ovarian syndrome, uterine leiomyomas and endometriosis: An update. *Gynecological Endocrinology* 2012; **28(3)**, 175-181.

[36] X He, Z Dong, Y Cao, H Wang, S Liu, L Liao, Y Jin, L Yuan and B Li. MSC-derived exosome promotes M2 polarization and enhances cutaneous wound healing. *Stem Cells International* 2019; **2019(1)**, 7132708.

[37] D Li, D Li, Z Wang, J Li, KA Shahzad, Y Wang and F Tan. Signaling pathways activated and regulated by stem cell-derived exosome therapy. *Cell & Bioscience* 2024; **14**, 105.

[38] M Hadidi, K Karimabadi, E Ghanbari, L Rezakhani and M Khazaei. Stem cells and exosomes: As biological agents in the diagnosis and treatment of polycystic ovary syndrome (PCOS). *Frontiers in Endocrinology* 2023; **14**, 1269266.

[39] F Tan, X Li, Z Wang, J Li, K Shahzad and J Zheng. Clinical applications of stem cell-derived exosomes. *Signal Transduction and Targeted Therapy* 2024; **9**, 17.

[40] P Hu, Q Yang, Q Wang, C Shi, D Wang, U Armato, ID Prà and A Chiarini. Mesenchymal stromal cells-exosomes: A promising cell-free therapeutic tool for wound healing and cutaneous regeneration. *Burns & Trauma* 2019; **7**, 38.

[41] D Bian, Y Wu, G Song, R Azizi and A Zamani. The application of mesenchymal stromal cells (MSCs) and their derivative exosome in skin wound healing: A comprehensive review. *Stem Cell Research & Therapy* 2022; **13**, 24.